

# Flow field Reconstruction for Inhomogeneous Turbulence using Data and Physics Driven Models

Aditya S. Ghate\*

*NASA Ames Research Center*

Sanjiva K. Lele†

*Stanford University*

## Abstract

A methodology combining Large Eddy Simulation (LES) trained data and a physics driven wavepacket model to obtain a reduced order reconstruction for broadband, three-dimensional, temporally stationary but spatially inhomogeneous, incompressible turbulence. Wake turbulence generated by an axisymmetric dragging disk with a turbulent co-flow serves as the benchmark test case. We begin by studying the proper-orthogonal decomposition of the turbulent fluctuations taken from a high-resolution LES to first identify whether the fields demonstrate a *low-rank* character. It is argued that the presence of the turbulent co-flow results in a largely broadband character lacking any tonal properties. This is especially true for Strouhal numbers greater than 1 and only a small fraction of energy is contained in the leading order Kelvin-Helmholtz modes. As such reconstructions and reduced order modeling purely relying on data from LES does not appear to be a lucrative solution - contrary to problems with strongly tonal character. To supplement the missing energy from a low order truncated mode expansion, we utilize a physics based super-resolution (enrichment) algorithm that relies on spatio-temporally localized Gabor wavepackets whose time evolution is described using a set of ordinary differential equations. The reconstructed flow has single- and two-point correlations that are consistent with the reference high-resolution simulation data.

## 1 Introduction

Many computational problems involving turbulent flows are characterized by figures of merit that in large part rely on a numerical simulation's ability to resolve a large range of spatio-temporal scales. Some examples include the study of scalar dispersion in atmosphere[1–3] and investigation of unsteady loading in wind turbines and wind farms[4, 5]. Examples in engineering include applications where aero-acoustics is of relevance such as airframe/landing gear noise[6] and jet noise[7, 8]. While the subject of reduced order modeling and reconstruction of mean flow has matured substantially over the past few decades[9–12], very limited progress has been made in reconstruction of fluctuations. The scope of this paper is to discuss the potential of data-driven modeling for temporally stationary, but spatially inhomogeneous turbulence fluctuations. It is argued that obtaining large bandwidth fluctuations using purely data driven approaches is likely impractical - due to slow convergence of the discovered modes as well as the need for large amount of high resolution data which is computationally expensive to generate. Physics driven modeling based on spatio-temporally localized wavepackets, *Gabor modes* can help mitigate shortcomings of the data driven model by providing highly accurate super-resolution for the data-driven model.

---

\*Science and Technology Corporation, aditya.s.ghate@nasa.gov

†Dept. of Aeronautics & Astronautics, Dept. of Mechanical Engineering, lele@stanford.edu

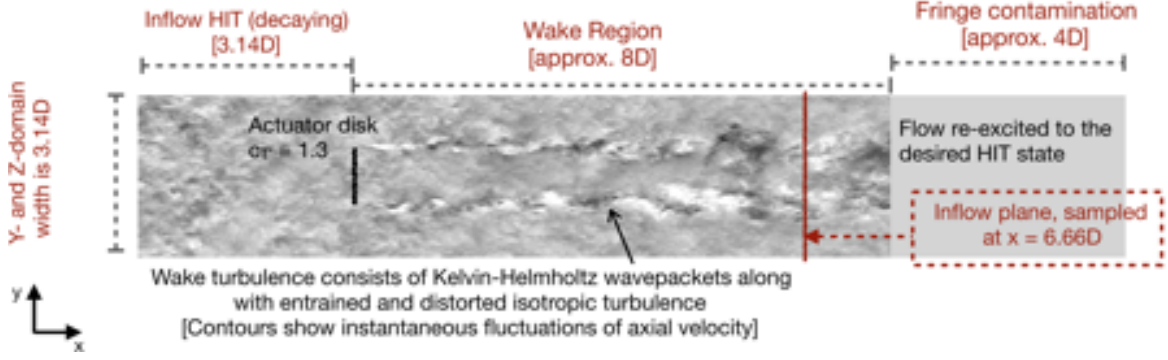


Figure 1: Problem configuration. Inflow homogeneous isotropic turbulence is generated using a concurrent forced HIT simulation with the desired integral length scale and dissipation rate.

## 2 Problem setup

We consider the problem of interaction between homogeneous isotropic turbulence advected by a uniform mean-flow, and a dragging actuator disk at a fixed thrust coefficient. The schematic of the problem set up is shown in Figure 1. This problem was studied in detail by Ghate et al.[13] for a variety of different inflow turbulence intensities controlled via two parameters: a) turbulence dissipation rate, and b) integral length scale of the inflow turbulence. Present work focuses on inflow based on Case 10 described in that work - this corresponds to an integral length scale of roughly 25% of the actuator disk diameter. Fully periodic domains are used enabling the utilization of a fully spectral (Fourier collocation with 2/3rd dealiasing) discretization along with an RK4 time-stepping scheme. A concurrent simulation of forced homogeneous isotropic turbulence is run which serves as the inflow for the domain of interest; the fringe method of Nordstom et al. [14] is used. The simulation is performed at the  $Re \rightarrow \infty$  limit and as such a subgrid scale model[15] is used to capture the loss of energy to subfilter scales.

The analysis and modeling presented in the remainder of this paper focuses on data extracted on a single transverse ( $y$ - $z$  plane) located  $6.66D$  units downstream of the actuator disk.

## 3 Modal representation of wake turbulence

The present work addresses the reconstruction problem for spatially inhomogeneous but temporally stationary turbulence by proposing a reconstruction of the turbulent flow field on an arbitrary ( $y - z$ ) plane as

$$\mathbf{u}(y, z, t) = \overline{\mathbf{U}}(y, z) + \mathbf{u}^{\text{SPOD}}(y, z, t) + \mathbf{u}^{\text{gab}}(y, z, t), \quad (1)$$

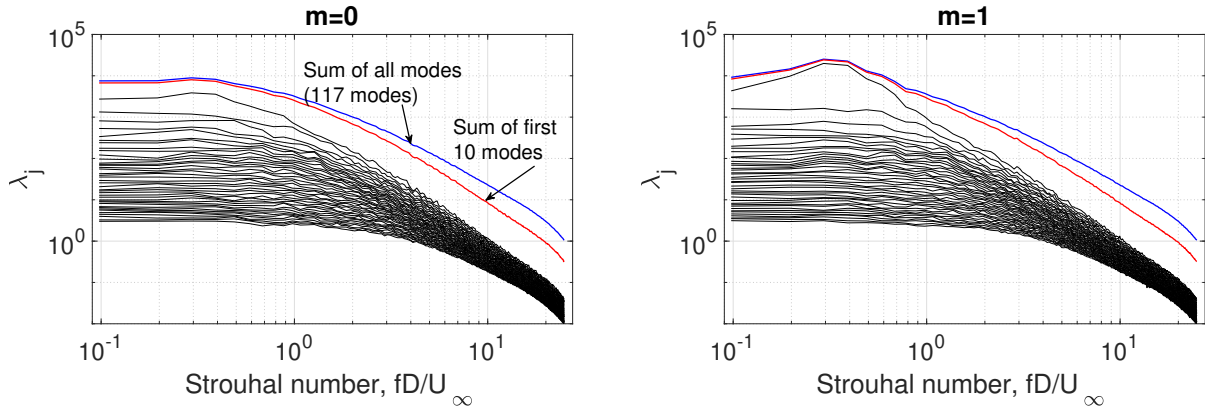
where  $\overline{\mathbf{U}}$  is the mean velocity (not the focus of present work), while  $\mathbf{u}^{\text{SPOD}}$  and  $\mathbf{u}^{\text{gab}}$  are portions of the velocity field that are represented using SPOD and Gabor modes, respectively.

### 3.1 Spectral Proper Orthogonal Decomposition

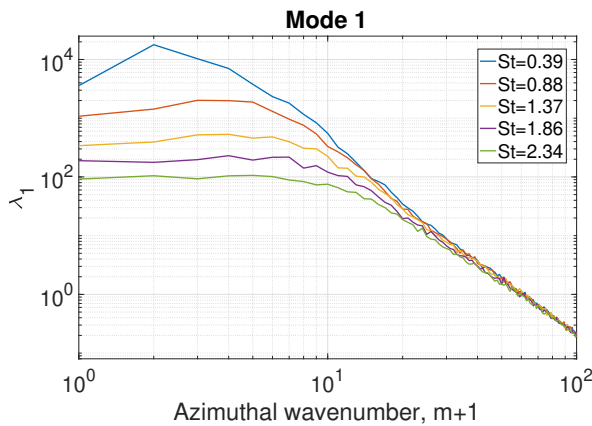
The flow field sampled on the  $y-z$  plane located  $6.66D$  downstream from the actuator disk is first decomposed into an ordered set of orthogonal SPOD modes in polar coordinates ( $r - \theta$ ):

$$\hat{\mathbf{u}}(r, m, f) = \frac{1}{N_T M_\theta} \sum_{n=0}^{N_T} \sum_{j=0}^{M_\theta} \mathbf{u}(r, \theta_j, t_n) e^{i(m\theta_j + 2\pi f t_n / T)} = \sum_{j=1}^J a_j(m, f) \Psi_j(r, m, f), \quad (2)$$

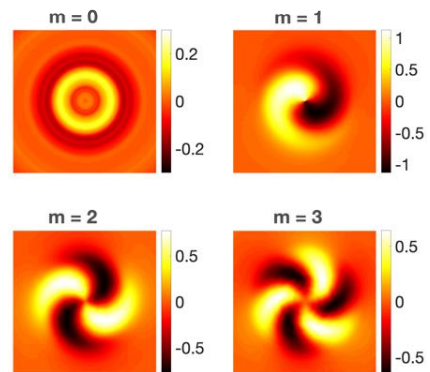
where  $\Psi_j(r, m, f)$  is the SPOD mode shape (in  $r$ ) corresponding to the  $m^{\text{th}}$  azimuthal wavenumber at a discrete frequency,  $f$ . The total number of modes,  $J$ , at each frequency-wavenumber pair is controlled by the number of realizations used to compute the SPOD modes, with each realization defined over a finite



(a) First 40 modes as a function of  $St$  and  $m$



(b)  $\lambda_j$  vs.  $m$



(c)  $\text{Re}\{\psi_{ux}(y, z, St = 0.39, m, j = 1)\}$

Figure 2: Modal energies and shapes for SPOD of wake turbulence taken at a transverse plane located  $6.66D$  downstream for the drag disk

sampling interval,  $T = 5.12D/U_\infty$  discretized uniformly using  $N_T$  sampling points (time steps). We take  $J = 117$  and  $M_\theta = 768$  (to avoid aliasing) in what follows; our numerical experiments with different choices of  $J$  and  $T$  showed that the most energetic wavepackets associated with the Kelvin-Helmholtz instability were adequately captured using this sampling. The modes are sorted according to their modal energy,  $\lambda_j(m, f) = \langle a_j^*(m, f)a_j(m, f) \rangle$ , which defines the contribution of each mode to the total kinetic energy of the flow. The modal energies and mode shapes are shown in Figure 2 up to a Strouhal number of 25. The Strouhal number corresponding to the Nyquist frequency of the temporal sampling is approximately 50; the upper half of the frequency range is excluded for the present analysis to avoid spurious artifacts associated with numerical/discretization error and spatial dealiasing.

Figure 2a, which shows the modal energies as a function of Strouhal number, suggests that a truncated representation consisting of the first 10 leading modes (and all values of  $m$ ) is only likely to produce accurate second order correlations for  $St < 1$ . Furthermore, at the axial downstream location being considered ( $6.66D$ ), we do not observe any dominant tone (frequency) in the primary varicose mode ( $m = 0$ ). Figure 2b suggests that there is substantially more energy in the  $m = 1$  mode compared to the  $m = 0$  mode, especially at low Strouhal numbers ( $St < 1$ ). It is also interesting to see that high wavenumbers do contain a substantial amount of energy as shown in Figure 2b; the energy decays only as a power law, as a function of the azimuthal wavenumber,  $m$  (see Figure 2b). The mode shapes shown in Figures 2c suggest that the bulk of the energy in the low order modes (small  $m$  and  $j$ ) at lower frequencies corresponds to the shear layer turbulence. The azimuthal homogeneity embedded by the Fourier representation in  $\theta$  is very efficient at isolating the shear-layer/inflectional turbulence from the free stream, including scales entrained

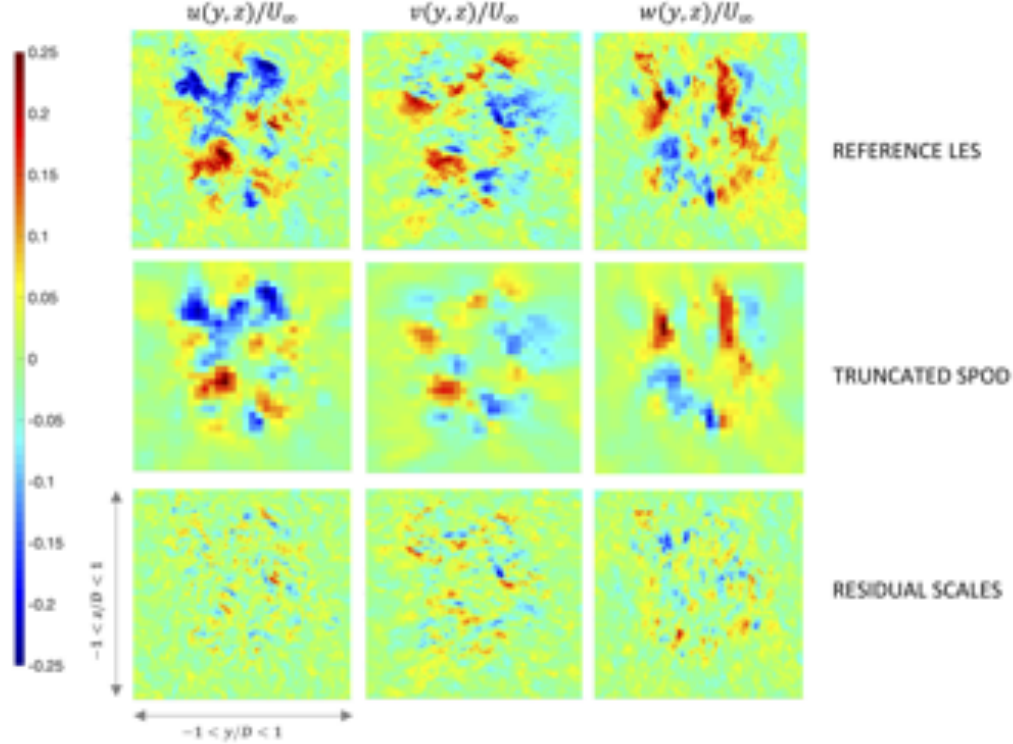


Figure 3: Decomposition of instantaneous flow (evaluated on a  $180 \times 180$  grid) into truncated SPOD representation (evaluated on a  $36 \times 36$  grid) and the resulting residual fields (evaluated on a  $180 \times 180$  grid) at an arbitrary sampling time. The velocity components in the Cartesian frame are obtained using an SPOD expansion truncated at  $m_{max} = 30$ ,  $j_{max} = 15$  and  $f_{max} = 1.4$ .

and subsequently distorted by the mean shear in the wake. Finally, an important consequence of finiteness of the data available to compute this modal representation is the uncertainty associated with higher order modes, since the overall representation only converges as  $\sqrt{n_{\text{samples}}}$  [16], where  $n_{\text{samples}}$  can only be increased by running longer simulations. As such, while higher order (in both  $m$  and  $j$ ) modes do contain non-negligible amounts of energy, in order to estimate them, we need to run very long simulations on very high resolution numerical grids. In contrast, the lower order modes at low-Strouhal numbers can be obtained using few  $n_{\text{samples}}$  using a sufficiently accurate coarse grid simulation with a good subgrid scale closure.

### 3.2 Truncated SPOD

A truncated/filtered representation corresponds to the following expansion:

$$\mathbf{u}^{\text{trunc}}(y, z, t) = \mathcal{I}_{(r,\theta)}^{(y,z)} \left\{ \sum_{|f| < f_{max}} \sum_{|m| < m_{max}} \sum_{j < j_{max}} a_j(m, f) \Psi_j(m, f, r) e^{-i(m\theta + ft)} \right\} \quad (3)$$

where  $a_j(m, f)$  can be computed using the appropriate orthogonality relations [17], and  $\mathcal{I}_{(r,\theta) \rightarrow (y,z)}$  is the interpolation operator. We will take velocity  $\mathbf{u}^{\text{SPOD}}(y, z, t)$  in Equation 1 to be the truncated SPOD expansion,  $\mathbf{u}^{\text{trunc}}(y, z, t)$ .

The truncated description being considered in the remainder of the paper uses  $f_{max} = 1.4$  (Strouhal number),  $m_{max} = 30$  (azimuthal wavenumbers) and  $j_{max} = 15$  (leading modes); however, we note that all arguments presented here apply for arbitrary choices of truncation parameters as long as the large scale coherent motions, in this case related to the Kelvin-Helmholtz instability, are captured by the truncated SPOD expansion.

We can define a residual field,  $\mathbf{u}^{\text{res}}$  as

$$\mathbf{u}^{\text{res}}(y, z, t) = \mathbf{u}(y, z, t) - \mathbf{u}^{\text{trunc}}(y, z, t) \quad (4)$$

where  $\mathbf{u}$  is the instantaneous (fluctuating) component in the independent sample. Due to the orthogonality properties of the SPOD representation, it is easy to show that the total domain averaged Reynolds stresses are given as the following superposition:

$$\langle u_i u_j \rangle = \langle u_i^{\text{trunc}} u_j^{\text{trunc}} \rangle + \langle u_i^{\text{res}} u_j^{\text{res}} \rangle. \quad (5)$$

Figure 3 shows an example of such a representation using an arbitrary sample from the simulation that was not used to compute the modes,  $\Psi_j(m, f)$ . It is important to note that the truncated representation can be evaluated on a  $32 \times 36 \times 36$  Cartesian grid in  $(y-z-t)$  space without any aliasing, as opposed to a  $180 \times 180 \times 512$  grid needed for the full fluctuating field. These results indicate that the expansion given in Equation 3 serves as an excellent surrogate to isolate large-scale, space-time coherent flow features in the  $y-z-t$  domain being considered. Figure 3 clearly suggests that the residual scales are primarily fine scale features that also appear to display *quasi-homogeneity*, i.e. spatial homogeneity at length scales corresponding to the filtering length scale implied by the SPOD truncation. The profile of the residual single point correlations (Figure 6) further indicates that these small scales are devoid of major radial inhomogeneity, and hence can be interpreted as the scales corresponding to the distorted free stream turbulence.

## 4 Gabor mode enrichment

### 4.1 Stationary Gabor modes

In the present application, the temporal evolution equations (see Equations 2.16-2.22 in [18]) for each Gabor mode can be simplified substantially by neglecting the inter-scale *sweeping* in the planar directions ( $y$  and  $z$ ) since  $\frac{U_y + u_y^{\text{spod}}}{U_x + u_x^{\text{spod}}}, \frac{U_z + u_z^{\text{spod}}}{U_x + u_x^{\text{spod}}} \ll 1$ . The planar reconstruction region ( $y-z$ ) is decomposed into  $18 \times 18$  quasi-homogeneous regions, each seeded with 80 Gabor modes. Under these assumptions, each Gabor mode is simply assumed to be advected in the streamwise direction according to the local streamwise time averaged velocity (Taylor's Hypothesis) and hence we refer to these modes as *stationary Gabor modes*. The energy exchange between the mean and SPOD scales and Gabor modes is captured via the straining/distortion effect. The temporal evolution of each Gabor mode located at  $(y, z)$  carrying a complex valued velocity,  $\hat{\mathbf{u}}$ , and a real valued wavevector,  $\mathbf{k}$ , from time step  $N$  to  $N+1$  separated by  $\Delta_t$  can be summarized by the following four step procedure (see [18] for further details):

$$\begin{aligned} \hat{u}_i^* &= \exp(ik_x \bar{U}_x(y, z) \Delta_t) \hat{u}_i^N, \\ \hat{u}_i^{**} &= \left[ \delta_{ij} + \Delta_t \left( \left( \frac{2k_i^N k_m^N}{k_p^N k_p^N} - \delta_{im} \right) \frac{\partial U_m}{\partial x_j}(y, z, t) - \nu_t(k) (k_p^N k_p^N) \delta_{ij} \right) \right] \hat{u}_j^*, \\ k_i^{N+1} &= \left[ \delta_{ij} - \Delta_t \frac{\partial U_j}{\partial x_i}(y, z, t) \right] k_j^N, \\ \hat{u}_i^{N+1} &= \left[ \frac{k_i^{N+1} k_j^{N+1}}{k_m^{N+1} k_m^{N+1}} - \delta_{ij} \right] \hat{u}_j^{**}, \end{aligned} \quad (6)$$

where  $U_m(y, z, t) = \bar{U}_m + u_m^{\text{SPOD}}(y, z, t)$ . In Equation 6, the first stage corresponds to advection of enriched turbulence in the direction normal to the sampling inflow plane ( $y-z$ ) by the time averaged velocity. The second and third steps represent the straining of enriching small scales by the larger SPOD (and mean) scales and the modification of the wavevector is a forward Euler approximation to the Eikonal equation. Finally, the projection implied in the fourth step is primarily used to discretely impose the divergence-free constraint; since the second and third steps are forward Euler approximations to the governing ODEs (see [18]), they inherently possess a spurious divergence ( $\mathcal{O}(\Delta_t^2)$ ), which can be removed at virtually no additional computational cost. The time-step is chosen based on the smallest scale enriched ( $k_{\text{max}}$ ) and the advective velocity  $\bar{U}_x$ . The choice of  $k_{\text{max}}$  is rather arbitrary and based on the Nyquist criterion of the physical space

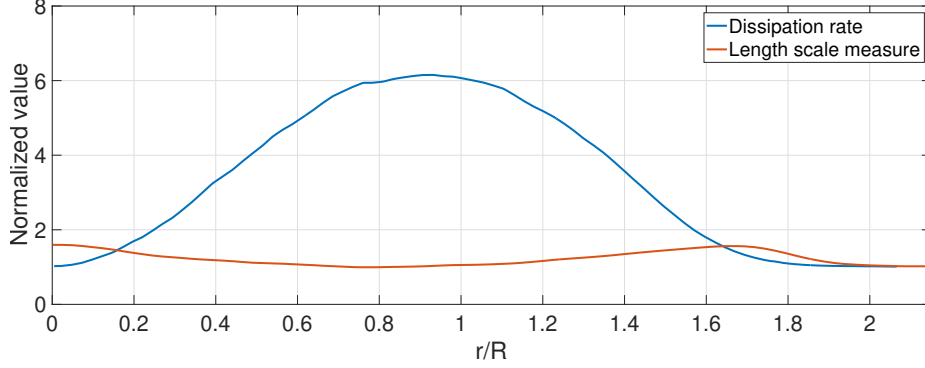


Figure 4: Model inputs used to generate stationary Gabor modes. Dissipation is normalized as  $\varepsilon(r)/\varepsilon(r \rightarrow \infty)$  and the length scale measure is normalized as  $L_{iso}(r)/L_{iso}(r \rightarrow \infty)$

numerical grid on which the enriched fields are rendered.

To initialize the Gabor modes in each quasi-homogeneous region, we begin by randomly sampling isotropic modes over log-spaced wavenumber-shells with a prescribed energy spectrum (see Equation 2.26a in [18]) parameterized using a dissipation rate,  $\varepsilon$ , and a length scale measure,  $L_{iso}$ ; both parameters vary only radially in the present application. The dissipation rate is modeled as

$$\varepsilon(r) = \varepsilon_\infty - \langle u_i^{\text{SPOD}} u_j^{\text{SPOD}} \rangle \frac{\partial \langle U_i \rangle}{\partial x_j}, \quad (7)$$

where  $\varepsilon_\infty$  is the dissipation rate of the turbulent co-flow (ambient/freestream) which is typically known or can be computed using a RANS model or an SGS model. The length scale measure is computed as

$$L_{iso}(r) = c_L \tau(r) [\langle U \rangle (r)], \quad (8)$$

where the constant  $c_L = 1/0.816$  ensures that  $L_{iso}(r \rightarrow \infty)$  corresponds to the integral length scale of the isotropic co-flow. The integral time scale,  $\tau$ , is computed as the integral time scale of the large scale axial velocity,  $u_x^{\text{spod}}$ . Figure 4 shows the profiles of the two model inputs as computed using the SPOD data. These isotropic modes are then distorted using the local mean velocity profile in accordance to Rapid distortion theory through a wavenumber-dependent time scale [18, 19] which results in anisotropic, small scale turbulence that is consistent with the mean velocity gradients in the quasi-homogeneous regions. An example description of this procedure is shown in [18] in the context of sheared boundary layer turbulence.

Once initialized, the dynamics represented by Equation 4.1 account for the following physical processes: a) rapid time-scale energy transfer from the large SPOD scales into the enriched small scales that occurs due to large scale strain, b) consistent temporal decorrelation of small-scales since this occurs primarily due to large scales *sweeping* enriched scales, c) effect of pressure as a Lagrange multiplier to impose the divergence free constraint (ensured by the Eikonal equation for  $\mathbf{k}$ ), and d) decay of the intense small-scale Burgers vortices generated by the non-local (in scale space) interactions of the straining term by representing the local interactions (in scale space) due to the non-linear relaxation as a spectral viscosity obtained using a Renormalization group (RNG) model [20].

Finally, it is important to emphasize the computational efficiency of the enrichment algorithm. The overall computational cost can be decomposed into two steps: a) temporal evolution of Gabor modes and b) rendering (transform into physical space). Log-spaced sampling of Gabor modes results in substantial compression in representing small scale turbulence (> 95% in 3D and > 20% in 2D) and the time advancement for each mode is an entirely local operation as detailed in Equation 4.1. The rendering step which is required to obtain the enriched velocity field on a numerical mesh requires a non-uniform Fast Fourier Transform (NUFFT); in the present application the cost of each 2D transform is equivalent to approximately 5-6 uniform 2D FFTs. Further details of the algorithm are provided in [21].

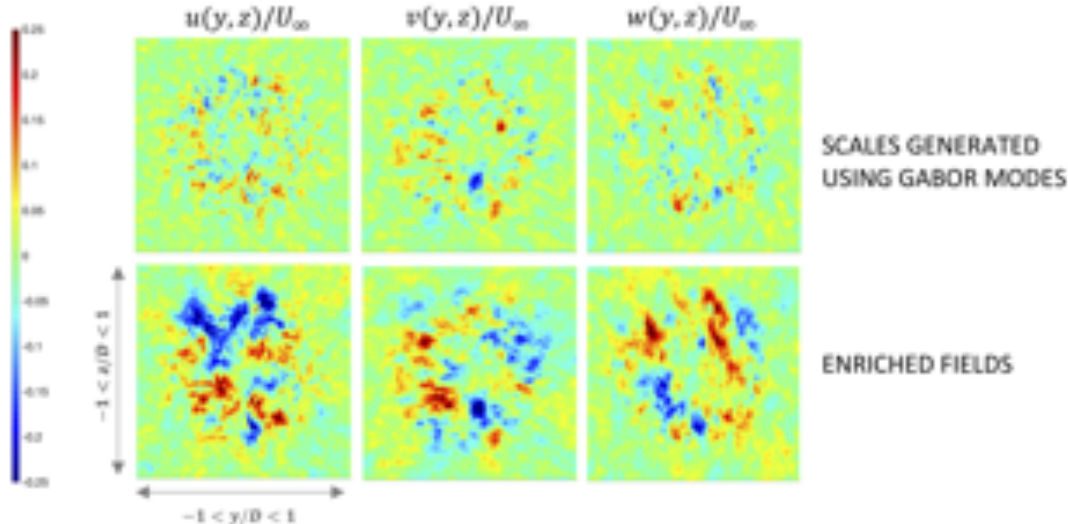


Figure 5: Instantaneous snapshot of enriched flow fields. Sample time is comparable with that in the representative snapshots shown in Figure 3.

While the application discussed in this paper focuses on planar reconstruction of wake turbulence, the use of Gabor modes for enrichment is more broadly applicable to a variety of three-dimensional complex flows, including wall-bounded turbulence. The algorithm requires some representation of domain/geometry-influenced large scales, either via a coarse LES [2] or other data-driven techniques such as deep neural networks [22], which explicitly influence the small-scale dynamics modelled by the Gabor mode representation of the flow. The choice of SPOD basis used in the present work to represent temporally stationary large scale flow physics is particularly convenient due to its orthogonality properties and spectrally sharp time-filtering of the truncated expansion.

## 4.2 Enrichment

Figure 5 shows an instantaneous snapshot of the inflow field taken at the same time as the one shown in Figure 3. A qualitative comparison of the Gabor mode induced fields with the residual fields suggests good overall agreement. Perhaps the one striking differentiating feature is the somewhat higher azimuthal imprinting in the Gabor mode induced instantaneous fields compared to the instantaneous residual fields (see Figure 3). While the small scales induced by the Gabor modes are indeed coupled with the truncated SPOD fields due to the localized straining (stage 2 in Equation 6), the overall azimuthal symmetry is a consequence of the model inputs, which only vary radially.

In order to facilitate more quantitative comparisons of the enriched field with the true full fields, several statistical measures are shown in Figure 6 through Figure 8. Figure 6 shows the single point correlations computed for the Gabor mode induced and residual fields, time and ensemble averaged. While the number of ensembles used for the residual fields is not sufficiently large to fully converge the statistics, the primary purpose of this figure is to demonstrate that an  $18 \times 18$  grid of Cartesian quasi-homogeneous regions on the  $y - z$  plane is sufficient to obtain the expected azimuthal symmetry in statistics. Fewer quasi-homogeneous regions would result in reduced spatial localization for the induced flow fields.

Assuming azimuthal symmetry, single point correlations as a function of radial location are shown in Figure 7. While the truncated SPOD expansion significantly under predicts the correlations, the Gabor-mode-enriched field shows excellent statistical agreement with the original field. Through the bulk of the shear layer, the physical anisotropy ( $\langle u_x u_r \rangle$ ) is well captured by the Gabor modes; the slight under-prediction of the turbulent kinetic energy at the shear layer centerline is notable. Upon closer inspection of the model inputs, we can explain this deficiency in terms of the estimated dissipation rate in Equation 7. This definition predicts  $\varepsilon(r = 0) = \varepsilon(r \rightarrow \infty)$  which appears to be a substantial under-prediction. In this model, the core

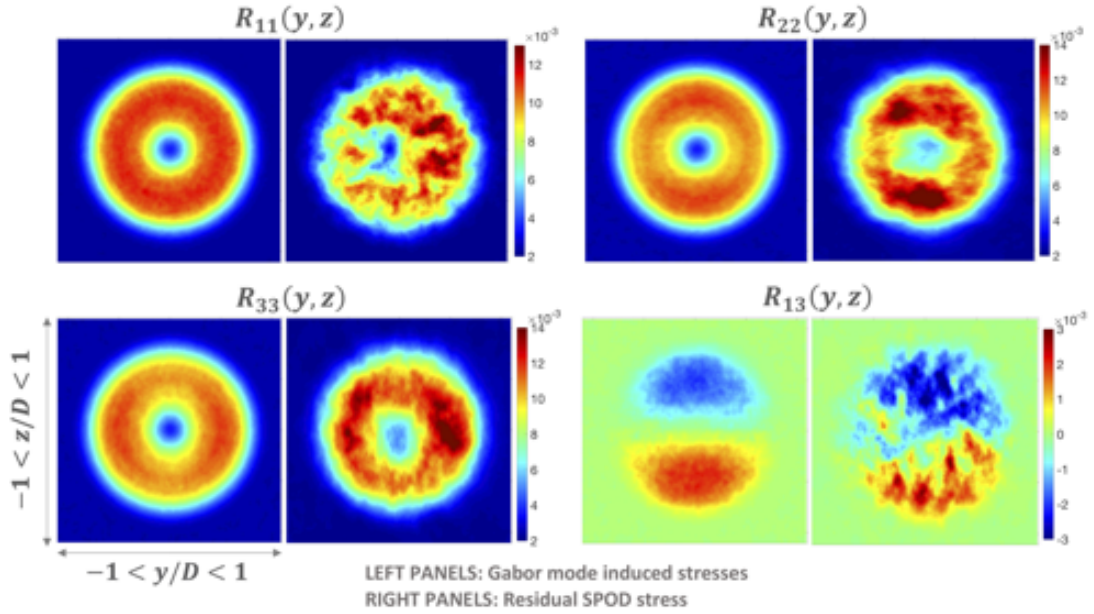


Figure 6: Time and ensemble averaged contours of single point small-scale second order correlations. The panels on the left correspond to covariances obtained for the Gabor mode enriched velocities (fields shown in the top panel of Figure 5) and the panels on the right correspond to covariances obtained for the residual scales (fields shown in the bottom panel of Figure 4).

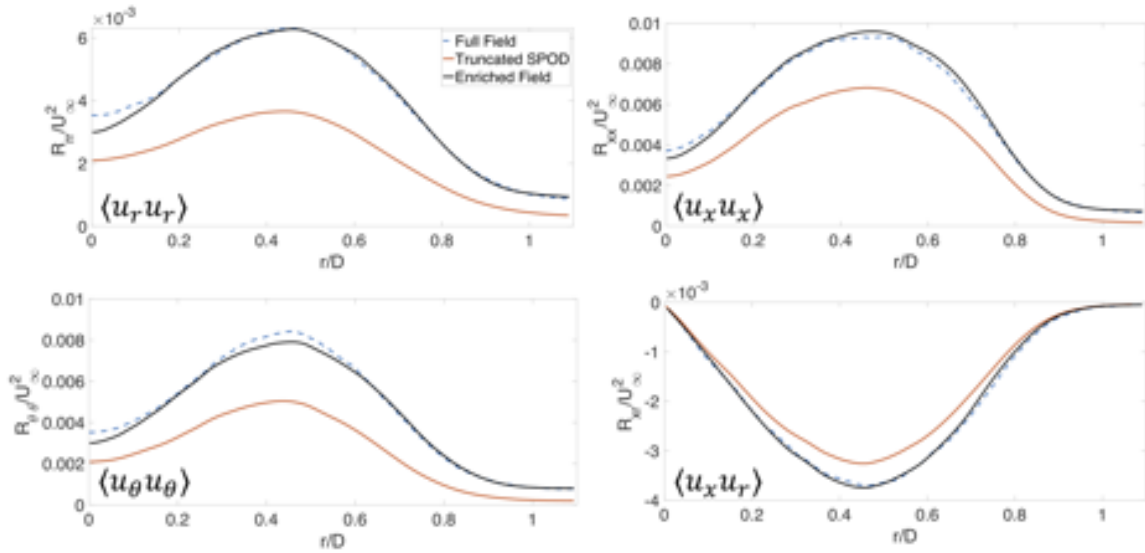


Figure 7: Single point correlations for the enriched fields

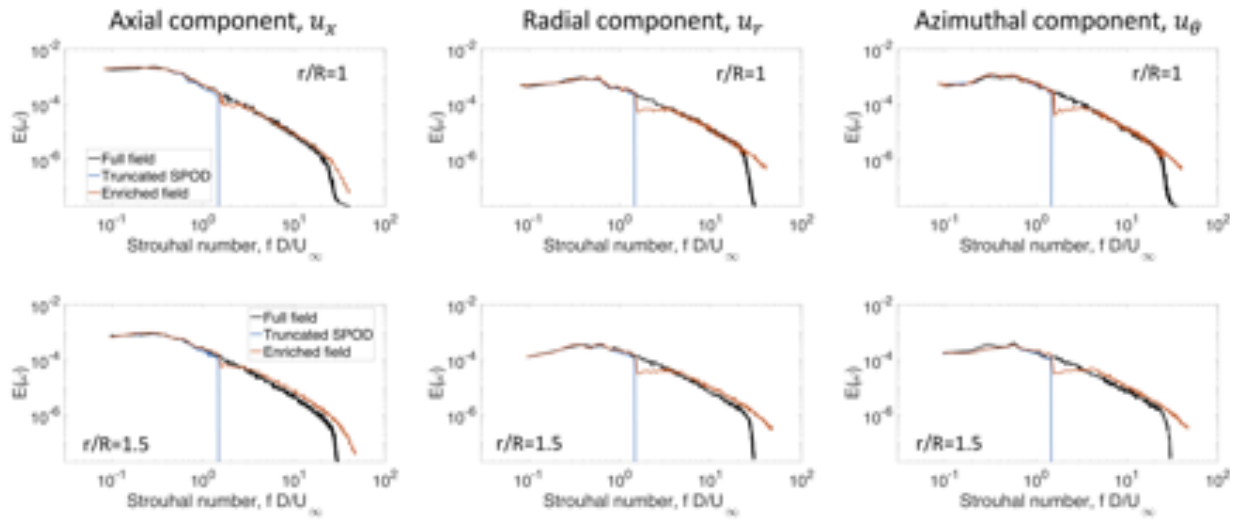


Figure 8: Temporal auto-spectra for the three velocity components extracted at two radial locations of  $r/R = 1$  and  $1.5$  where  $R$  is the radius of the wake-generating actuator disk.

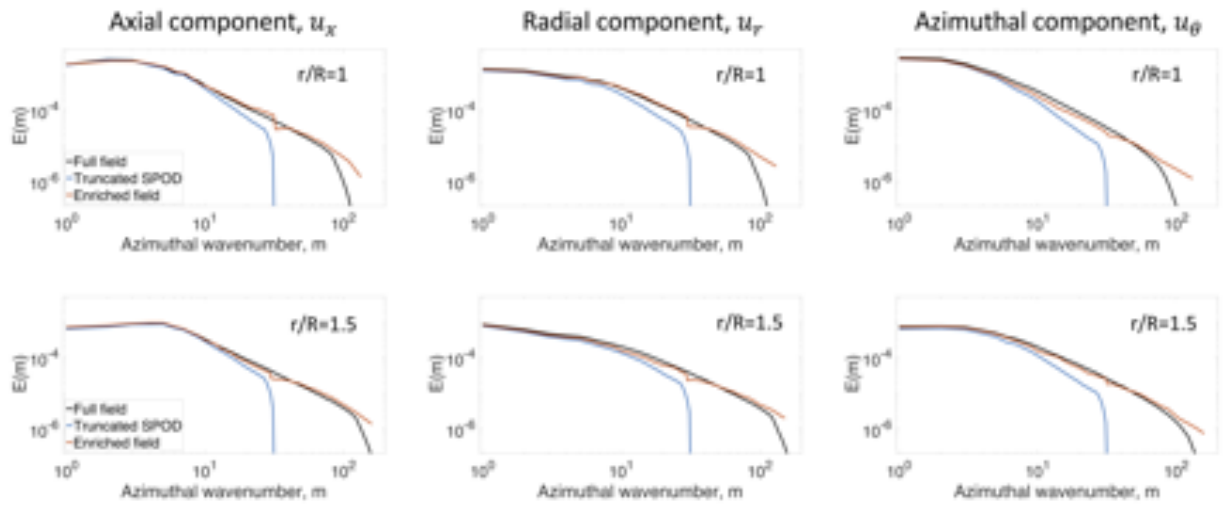


Figure 9: Azimuthal auto-spectra for the three velocity components extracted at two radial locations of  $r/R = 1$  and  $1.5$  where  $R$  is the radius of the wake-generating actuator disk.

turbulence entrained by the shear layer is not neglected. Since  $E(k) \propto \varepsilon^{2/3}$ , any underprediction of the dissipation rate results in underprediction of variances.

The 1D power spectra in frequency (Strouhal number) and azimuthal wavenumber ( $m$ ) are shown for the velocity components in Figures 8 and 9 at two different radial locations. These spectra further corroborate the effectiveness of the current approach. It is interesting to note from Figure 9 that the enrichment using Gabor modes leads to an increase in energy for  $m < 30$ , since it is able to generate smaller azimuthal scales that are truncated due to filtering in time and radial direction in the truncated expansion. Further discussion of 1D spatial spectra in the context of subfilter-scale enrichment can be found in [21] for highly anisotropic near-wall turbulence.

Overall, our results show that spatially inhomogeneous turbulent flows can be effectively reconstructed by combining a few SPOD modes to capture the energy containing coherent modes, which capture the large scale inhomogeneity, enabling enrichment using Gabor modes. While in [18], Gabor mode enrichment was assessed on wall-bounded turbulent flows using filtered LES data, it is promising to note the ability of the algorithm to accurately provide enrichment for a more conventional data-driven reduced order modeling algorithm. A potential step towards future improvement is to address the energy deficiency that is seen in azimuthal and radial velocity components, near the cutoff frequency of the truncated SPOD reconstruction ( $St = 1.4$ ). This is a consequence of an inconsistency between the *geometric anisotropy* implied by the resulting quasi-homogeneous regions (parameterized by  $F_{co}$ ) and the true Reynolds stress anisotropy of the subfilter scales. For the present choice of  $F_{co} = 1.4$ , the resulting aspect ratio of the  $[t, y, z]$  quasi-homogeneous regions is rather skewed ( $\approx [5 \times 1 \times 1]$ ); this can be mitigated by a Reynolds-stress informed choice of  $F_{co}$ .

## 5 Conclusions

A flow reconstruction method that combines data-driven modal analysis with physics-based turbulence enrichment is developed and tested for incompressible wake turbulence. For the actuator-disk wake considered in this paper, the circumferential symmetry of the shear layer is leveraged to represent the shear-layer driven turbulence using a compressed set of SPOD modes. The orthogonality of SPOD modes allows us to interpret such a truncated representation as a filtering operation which subsequently enables generation of *subfilter* scales via Gabor mode enrichment. This juxtaposition of data-driven modeling with physics-based enrichment enables efficient representation of statistically stationary flow fields that contain both large-scale coherent motions associated with inflectional instabilities and broadband  $k^{-5/3}$  turbulence. Hence, the coupled formulation is more broadly applicable to a variety of statistically stationary turbulent flows including wall-bounded turbulence. We further emphasize that once the SPOD mode shapes are determined using data, an arbitrarily large number of random ensembles of statistically equivalent flow realizations can be generated via randomizing the phase of the complex valued amplitudes,  $a_j(m, f)$  in Equation 3. Each of these random realizations can be further enriched on-the-fly with smaller scales using randomly sampled Gabor modes, which provide a consistent extrapolation of the spectral content present in the SPOD representation. This procedure could be useful for generating ensembles of statistically equivalent inflow conditions containing both inhomogeneous large scale and homogenous small scales motions.

## Acknowledgements

SKL acknowledges partial support from NSF-CBET-1803378. All simulations were performed on Stampede2 supercomputer under the XSEDE project ATM170028. ASG was funded by Tomkat Center for Sustainable Energy during his time at Stanford University and by the T<sup>3</sup> program at NASA Ames Research Center.

## References

- [1] John D Wilson and Brian L Sawford. Review of lagrangian stochastic models for trajectories in the turbulent atmosphere, 1996.

- [2] Eliot W Quon, Aditya S Ghate, and Sanjiva K Lele. Enrichment methods for inflow turbulence generation in the atmospheric boundary layer. In *Journal of Physics: Conference Series*, volume 1037, page 072054. IOP Publishing, 2018.
- [3] Dunhui Xiao, CE Heaney, L Mottet, F Fang, W Lin, IM Navon, Y Guo, OK Matar, AG Robins, and CC Pain. A reduced order model for turbulent flows in the urban environment using machine learning. *Building and Environment*, 148:323–337, 2019.
- [4] Aditya S Ghate and Sanjiva K Lele. A modeling framework for wind farm analysis: wind turbine wake interactions. In *33rd Wind Energy Symposium*, page 0725, 2015.
- [5] Paula Doubrawa, Jennifer R Annoni, Jason M Jonkman, and A Ghate. Optimization-based calibration of fast. farm parameters against large-eddy simulations. In *2018 Wind Energy Symposium*, page 0512, 2018.
- [6] Man Long Wong, Gaetan K. Kenway, Aditya S Ghate, Gerrit-Daniel Stich, and Cetin C Kiris. Predictions of lagoon nose landing gear flow and noise using wall-modeled large eddy simulations. In *28th AIAA/CEAS Aeroacoustics 2022 Conference*, page 2850, 2022.
- [7] Gerrit-Daniel Stich, Jeffrey A Housman, Aditya S Ghate, and Cetin C Kiris. Jet noise prediction with large-eddy simulation for chevron nozzle flows. In *AIAA Scitech 2021 Forum*, page 1185, 2021.
- [8] Gerrit-Daniel Stich, Aditya S Ghate, Jeffrey A Housman, and Cetin C Kiris. Wall modeled large eddy simulations for nasa’s jet noise consensus database of single-stream, round, convergent jets. In *AIAA SCITECH 2022 Forum*, page 0684, 2022.
- [9] David Amsellem and Charbel Farhat. An online method for interpolating linear parametric reduced-order models. *SIAM Journal on Scientific Computing*, 33(5):2169–2198, 2011.
- [10] Kyle M Washabaugh, Matthew J Zahr, and Charbel Farhat. On the use of discrete nonlinear reduced-order models for the prediction of steady-state flows past parametrically deformed complex geometries. In *54th AIAA Aerospace Sciences Meeting*, page 1814, 2016.
- [11] Mateus Dias Ribeiro, Abdul Rehman, Sheraz Ahmed, and Andreas Dengel. Deepcfd: Efficient steady-state laminar flow approximation with deep convolutional neural networks. *arXiv preprint arXiv:2004.08826*, 2020.
- [12] Abhijit Uday Kurtakoti and Satyadhyan Chickerur. Steady flow approximation using capsule neural networks. In *2020 IEEE Sixth International Conference on Multimedia Big Data (BigMM)*, pages 257–261. IEEE, 2020.
- [13] Aditya S Ghate, Niranjana Ghaisas, Sanjiva K Lele, and Aaron Towne. Interaction of small scale homogeneous isotropic turbulence with an actuator disk. In *2018 Wind Energy Symposium*, page 0753, 2018.
- [14] Jan Nordström, Niklas Nordin, and Dan Henningson. The fringe region technique and the fourier method used in the direct numerical simulation of spatially evolving viscous flows. *SIAM Journal on Scientific Computing*, 20(4):1365–1393, 1999.
- [15] Franck Nicoud, Hubert Baya Toda, Olivier Cabrit, Sanjeeb Bose, and Jungil Lee. Using singular values to build a subgrid-scale model for large eddy simulations. *Phys. Fluids*, 23(8):085106, 2011.
- [16] Peter Welch. The use of fast fourier transform for the estimation of power spectra: a method based on time averaging over short, modified periodograms. *IEEE Transactions on audio and electroacoustics*, 15(2):70–73, 1967.
- [17] Aaron Towne, Oliver T Schmidt, and Tim Colonius. Spectral proper orthogonal decomposition and its relationship to dynamic mode decomposition and resolvent analysis. *Journal of Fluid Mechanics*, 847:821–867, 2018.

- [18] Aditya S Ghate and Sanjiva K Lele. Subfilter-scale enrichment of planetary boundary layer large eddy simulation using discrete fourier–gabor modes. *J. Fluid Mech.*, 819:494–539, 2017.
- [19] Jakob Mann. The spatial structure of neutral atmospheric surface-layer turbulence. *Journal of fluid mechanics*, 273:141–168, 1994.
- [20] VM Canuto and MS Dubovikov. A dynamical model for turbulence. i. general formalism. *Physics of Fluids*, 8(2):571–586, 1996.
- [21] Aditya Suresh Ghate. *Gabor Mode Enrichment in Large Eddy Simulation of Turbulent Flows*. PhD thesis, Stanford University, 2018.
- [22] PA Srinivasan, L Guastoni, Hossein Azizpour, PHILIPP Schlatter, and Ricardo Vinuesa. Predictions of turbulent shear flows using deep neural networks. *Physical Review Fluids*, 4(5):054603, 2019.